FINITE ELEMENT MODELING FOR HYDRODYNAMIC AND SEDIMENT TRANSPORT ANALYSIS (I) : HYDRODYNAMIC STUDY

Joon-Woo Noh

Department of Civil Engineering, Colorado State University, Ft. Collins, Colorado, 80523 USA

Abstract: In this study, using the numerical model, the flow motion around skewed abutment is investigated to evaluate the skewness effect on the flow distribution. The skewness angle of the abutment which make with main flow direction is changed from 30° to 150° with increments of 10° while the contraction ratios due to the abutment are kept constant. For the investigation of the combined effects on the relationship between the skewness angle and flow intensities, this process will be repeated for different types of abutment (single and double) with different flow intensities. The maximum velocities and the velocity distributions, which can be obtained from each angle, are examined and analyzed corresponding to different angles of inclination. Based on successive model applications, an empirical expression, given in a function of contracted ratio and skewness angle, is derived for relating velocity amplifications according to the angle variations.

Keywords: finite element method, Petrov-Galerkin, Skewness, abutment

1. INTRODUCTION

This study is to determine the flow distribution around skewed abutments. Most of abutment studies are done for flow analysis around perpendicular abutments; whereas studies on unsymmetrical skewed abutments are very limited. The analysis is done using the 2D finite element surface flow model which solves the Reynolds-averaged turbulent flow equations on a horizontal plane passing through the average water surface. In the formulations of the model, the vertical gradient effects are considered through the use of power law and the finite element upwind scheme is employed to reduce numerical oscillations which commonly occur in convection dominant flow.

For the treatment of numerical oscillations, the upwind finite element scheme has been proposed and applied. Heinrich et al. (1977) extended upwind approach to the two dimensional convection and diffusion equations. Brooks and Hughes (1982) presented the general framework on the upwind scheme for its application on the

Navier Stokes equation. Katopodes (1984) solved one and two-dimensional unsteady shallow wave equations employing dissipative Galerkin scheme. Berger and Stockstill (1995) produced a 2D finite element model using an extension of the SUPG (Streamline Upwind Petrov-Galerkin) concept for shallow water equation and applied their model to high velocity channels. Tisdale et al. (1998) applied streamline upwind scheme for overland flow.

Most of the past studies on the flow distributions around abutments are based on groins and dikes. Mayerle et al. (1995) using 3D finite element model compared reattachment length by applying different definitions of eddy viscosity closure. Ouillon and Dartus (1997) investigated flow around groins using three-dimensional k-ε model adopting porosity method to track the free surface. Molinas and Hafez (2000) derived formulations of velocity amplification factor according to the abutment contraction ratio using 2D finite element model.

2. MODEL DESCRIPTION

The governing equation is composed of continuity and momentum equations

$$\frac{\partial u}{\partial x}+\frac{\partial v}{\partial y}=0 \tag{1}$$

$$u\frac{\partial u}{\partial x}+v\frac{\partial u}{\partial y}=-\frac{\partial}{\partial x}\left(\frac{P}{\rho}\right)+\frac{\partial}{\partial x}\left(2\nu_T\frac{\partial u}{\partial x}\right)+\frac{\partial}{\partial y}\left[\nu_T\left(\frac{\partial u}{\partial y}+\frac{\partial v}{\partial x}\right)\right]+\left[\frac{\partial}{\partial z}\left(\frac{\tau_s}{\rho}\right)\right]_{z=H}+F_x \tag{2}$$

$$u\frac{\partial v}{\partial x}+v\frac{\partial v}{\partial y}=-\frac{\partial}{\partial y}\left(\frac{P}{\rho}\right)+\frac{\partial}{\partial x}\left[\nu_T\left(\frac{\partial u}{\partial y}+\frac{\partial v}{\partial x}\right)\right]+\frac{\partial}{\partial y}\left(2\nu_T\frac{\partial v}{\partial y}\right)+\left[\frac{\partial}{\partial z}\left(\frac{\tau_n}{\rho}\right)\right]_{z=H}+F_y \tag{3}$$

where, u is the flow velocity in the x-direction (longitudinal); v is flow velocity in the y- direction (lateral); P is the mean pressure; ν_T is the turbulent viscosity; $F_x=g\sin\delta$ and $F_y=0$ are body forces in the longitudinal and lateral direction respectively; g is the gravitational acceleration; δ is averaged water surface slope in the longitudinal direction of flow; z is vertical distance from the channel bed; H is averaged flow depth; ρ is the density of water; τ_s and τ_n are the longitudinal and lateral turbulent shear stresses respectively.

The two shear stress terms which appear in Eq. (2) and (3) are evaluated at the water surface.

$$\frac{\tau_S(z)}{\rho}=\nu_T\frac{\partial u}{\partial z};\qquad \frac{\tau_n(z)}{\rho}=\nu_T\frac{\partial v}{\partial z} \tag{4}$$

Assuming a power law variation of the longitudinal velocity in the vertical direction, a general relationship can be shown as

$$\frac{u(z)}{U_{av}}=C_1\left(\frac{z}{H}\right)^{C_2} \tag{5}$$

where, C_1, C_2 are experimental coefficients de scribing vertical velocity distributions; $u(z)$ is longitudinal local velocity as a function of ver tical distance from the bed; U_{av} is depth- aver aged longitudinal velocity; According to Toffeletti (1963), for large rivers, C_1 and C_2 values are found to be 1.15, and 0.15 respectively or usually,

$$C_1=1+\frac{1}{\kappa}\sqrt{\frac{f}{8}},\ \text{and}\ \ C_2=\frac{1}{\kappa}\sqrt{\frac{f}{8}} \tag{6}$$

Assuming a parabolic distribution, the vertical variation of the turbulent viscosity can be given as

$$\nu_T(z)=\kappa V_*z\left(1-\frac{z}{H}\right) \tag{7}$$

In which $V_* = \sqrt{gRS_E}$ shear velocity, R is the hydraulic radius, S_E is energy gradient slope. Substituting Eq. (4) through (7) into the term which defines the vertical variation of the longitudinal shear stress terms in Eq. (2) can be expressed in terms of the surface velocity u and v, the Darcy-Weisbach friction factor f, and von Karman constant κ as

$$\left(\frac{\partial}{\partial z}\left(\frac{\tau_s}{\rho}\right)\right)_{z=H} = -C_1 C_2 \frac{\kappa}{H}|u|u\sqrt{\frac{f}{8}} \tag{8}$$

From the isotropic turbulent viscosity assumption, the depth-averaged turbulent viscosity can be obtained by integrating Eq. (7) over flow depth as (Laufer, 1951; Rastogi & Rodi, 1978):

$$\nu_T = 0.0765 H V_* \tag{9}$$

2.1 Petrov-Galerkin Finite Element Scheme

While the weighting function of the standard Galerkin method is identical to the shape function, the weighting function of the Petrov-Galerkin scheme is given by Zienkiwicz (1989) as

$$W_i = N_i + \frac{\alpha \bar{h}}{2|\mathbf{V}|}\left(u\frac{\partial N_i}{\partial x} + v\frac{\partial N_i}{\partial y}\right) \tag{10}$$

where, $\alpha = \coth\frac{\gamma}{2} - \frac{2}{\gamma}$, and γ is the cell Reynolds number given by

$$\gamma = \mathrm{Re}|\mathbf{V}|\bar{h} \tag{11}$$

in which, W_i is a weighting function; N_i is a shape function; Re is Reynolds number; α is an upwind coefficient; and $\bar{h}$ is element length. The upwind coefficient α varies according to the Reynolds number from 0 to 1. When $\alpha = 0$, the equation will be identical to the standard Galerkin equation, when $\alpha = 1$, then fully upwind equation is obtained. The mean pressure P appears in the governing equations can be computed using the penalty function as

$$P^{(n)} = P^{(n-1)} - \lambda\left(\frac{\partial u}{\partial X} + \frac{\partial v}{\partial Y}\right) \tag{12}$$

where, λ is the penalty coefficient.

The advantage of this approach is not only to reduce the number of variables but also to satisfy the continuity equation automatically without solving any additional equations. In the model, the mixed interpolation scheme is used to find P in which a lower order of interpolation is used for a pressure than for the velocity components.

3. MODEL VERIFICATION

Experimental field data for flow distribution around skewed abutments are very limited. One such experimental data set is collected by Kwan (1984). Kwan evaluates the abutment skewness effect on the maximum scour hole depth around abutment nose using 4 different contraction ratios with angle variations of 45°, 90°and 135° (Fig. 1a).

Since the major factor affecting the scour depth is the magnitude of flow velocity, the maximum scour is expected to take place at a location where the maximum velocity occurs. For model verification, Kwan's experiments with $L/B = 0.3$ and $U_{app}/V_* = 12$, have been simulated by changing the inclination of model abutments between 30°and 140° by 10° increments where, L is abutment length in x-direction B is abutment height, and U_{app} is the approach velocity from channel inlet. The computed results are presented to show maximum nose velocities against various skewness angles in Fig.

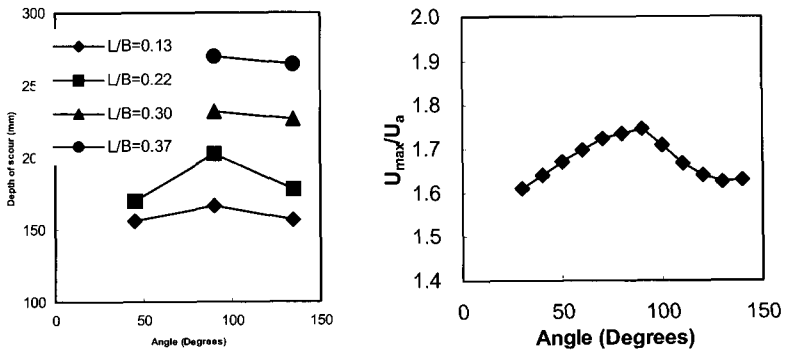

Fig. 1 Comparison between experimental and numerical results: (a) Kwan (1984) Experiments; (b) Numerical Simulation for L/B=0.3 and U_{app}/V_*=12.

1(b). The model used in this study predicts maximum velocity for the 90° case. Based on the assumption that the flow velocity is proportional to the scour depth, this finding shows good agreement with Kwan (1984)'s experimental results.

4. MODEL APPLICATION

4.1 Single Abutment

A series of computer simulation runs has been conducted to study the angle variation effects. The skewness angle has been changed by 10° increments while keeping a 30% contraction ratio, σ, into the flow. The skewness angle varies between 30° and 150° to avoid secondary effects due to the abutment length. The finite element mesh is provided using 4080 elements with 4239 nodal points. Fig. 2 shows the typical velocity distributions of the single abutment case with skewness angle. For comparison, each maximum velocity according to the angle variation is chosen along the observation lines at the upstream, mid-point, and downstream end of the abutment. In Fig. 2, each observation line is indicated using thick lines in the vicinity of the abutment along with the finite element mesh

The maximum velocities obtained from each run along the observation lines are listed in Table 1. These results show that maximum velocity proportionally increases with the skewness angle up to 90°; for skewness angle between 90° and 130°, the maximum nose velocity decreases with increasing skewness.

4.2 Double Abutments

The second series of simulation were conducted using pairs of abutments. For this portion of study, a new mesh is constructed using 3440 elements with 3574 nodal points. The abutment and the observation lines along the abutment are allowed to vary with respect to the angle of inclination, while keeping the same projected contraction ratio of 30 %. The range of skewness angle variation was chosen from 50° to 130°. The total velocity $U_t\ (=\sqrt{u^2+v^2})$ distributions are computed along the observation lines which are indicated using thick lines to compare the lateral velocity profiles across the upstream, mid-point and downstream end of the abutment in Fig. 3. The maximum velocity results computed from the double abutment runs are given in Table 2.

Table 1. Resultant maximum velocities for single abutments

θ	Location	$f = 0.08$		$f = 0.02$		$f = 0.0088$	
		U_{max}/V_*	U_{max}/U_{app}	U_{max}/V_*	U_{max}/U_{app}	U_{max}/V_*	U_{max}/U_{app}
30°	Upstream	15.96	1.60	32.09	1.60	48.22	1.61
	Mid-Point	16.11	1.61	32.48	1.62	48.92	1.63
	Downstream	16.28	1.63	32.91	1.65	49.69	1.66
40°	Upstream	16.22	1.62	32.83	1.64	49.75	1.66
	Mid-Point	16.42	1.64	33.39	1.67	50.90	1.70
	Downstream	16.56	1.66	33.95	1.70	51.37	1.71
50°	Upstream	16.52	1.65	33.74	1.69	51.13	1.70
	Mid-Point	16.78	1.68	34.14	1.71	52.49	1.75
	Downstream	16.85	1.68	34.68	1.73	52.75	1.76
60°	Upstream	16.77	1.68	34.43	1.72	53.24	1.77
	Mid-Point	17.02	1.70	34.95	1.75	53.67	1.79
	Downstream	17.12	1.71	35.28	1.76	53.69	1.79
70°	Upstream	17.08	1.71	34.94	1.75	54.67	1.82
	Mid-Point	17.23	1.72	35.67	1.78	54.61	1.82
	Downstream	17.38	1.74	35.61	1.78	54.36	1.81
80°	Upstream	17.25	1.72	35.68	1.78	55.49	1.85
	Mid-Point	17.31	1.73	36.01	1.80	54.94	1.83
	Downstream	17.50	1.75	35.81	1.79	55.31	1.84
90°	Upstream	17.33	1.73	36.39	1.82	56.07	1.87
	Mid-Point	17.48	1.75	36.21	1.81	55.46	1.85
	Downstream	17.55	1.75	36.09	1.80	55.73	1.86
100°	Upstream	16.95	1.70	35.44	1.77	55.73	1.86
	Mid-Point	17.11	1.71	35.34	1.77	54.44	1.81
	Downstream	17.18	1.72	35.30	1.77	54.09	1.80
110°	Upstream	16.40	1.64	34.61	1.73	54.95	1.83
	Mid-Point	16.74	1.67	34.59	1.73	52.99	1.77
	Downstream	16.89	1.69	34.49	1.72	52.84	1.76
120°	Upstream	16.01	1.60	33.46	1.67	51.40	1.71
	Mid-Point	16.47	1.65	33.80	1.69	51.68	1.72
	Downstream	16.74	1.67	34.07	1.70	51.57	1.72
130°	Upstream	15.67	1.57	31.91	1.60	48.86	1.63
	Mid-Point	16.37	1.64	33.21	1.66	50.62	1.69
	Downstream	16.71	1.67	33.74	1.69	51.69	1.72
140°	Upstream	15.65	1.56	31.05	1.55	46.42	1.55
	Mid-Point	16.43	1.64	32.94	1.65	50.16	1.67
	Downstream	16.82	1.68	34.21	1.71	51.82	1.73
150°	Upstream	15.91	1.59	31.47	1.57	46.84	1.56
	Mid-Point	16.63	1.66	33.32	1.67	50.22	1.67
	Downstream	16.97	1.70	34.70	1.73	52.71	1.76

Table 2. Resultant maximum velocities for double abutments

°	Locations	f= 0.08		f= 0.02		f= 0.0088	
		U_{max}/V_*	U_{max}/U_{app}	U_{max}/V_*	U_{max}/U_{app}	U_{max}/V_*	U_{max}/U_{app}
50°	Upstream	14.40	1.44	29.14	1.46	45.69	1.52
	Mid-Point	14.30	1.43	28.80	1.44	45.37	1.51
	Downstream	14.21	1.42	28.79	1.44	45.39	1.51
60°	Upstream	15.18	1.52	31.79	1.59	49.07	1.64
	Mid-Point	15.08	1.51	31.33	1.57	47.97	1.60
	Downstream	15.06	1.51	31.20	1.56	48.14	1.60
70°	Upstream	15.98	1.60	33.55	1.68	51.67	1.72
	Mid-Point	15.90	1.59	33.00	1.65	50.86	1.70
	Downstream	15.88	1.59	32.90	1.65	50.66	1.69
80°	Upstream	16.77	1.68	34.98	1.75	53.55	1.78
	Mid-Point	16.76	1.68	34.67	1.73	53.33	1.78
	Downstream	16.82	1.68	34.46	1.72	53.42	1.78
90°	Upstream	17.19	1.72	35.84	1.79	54.56	1.82
	Mid-Point	17.51	1.75	35.89	1.79	54.77	1.83
	Downstream	17.52	1.75	35.99	1.80	54.85	1.83
100°	Upstream	16.25	1.63	33.59	1.68	51.34	1.71
	Mid-Point	16.97	1.70	34.52	1.73	52.43	1.75
	Downstream	17.19	1.72	34.66	1.73	52.26	1.74
110°	Upstream	15.12	1.51	30.99	1.55	47.61	1.59
	Mid-Point	16.23	1.62	32.88	1.64	50.02	1.67
	Downstream	16.65	1.66	33.42	1.67	50.57	1.69
120°	Upstream	13.70	1.37	28.07	1.40	42.23	1.41
	Mid-Point	15.35	1.54	30.87	1.54	46.69	1.56
	Downstream	16.07	1.61	31.88	1.59	48.40	1.61
130°	Upstream	12.24	1.22	22.46	1.12	36.41	1.21
	Mid-Point	14.34	1.43	27.24	1.36	42.82	1.43
	Downstream	15.37	1.54	29.42	1.47	45.22	1.51

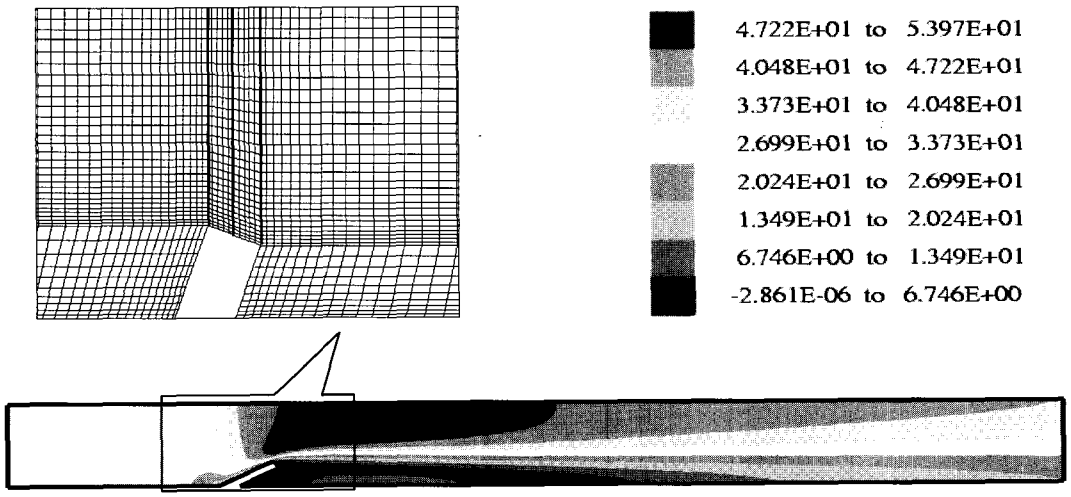

Fig. 2 Typical flow distributions and observation lines for single abutment cases

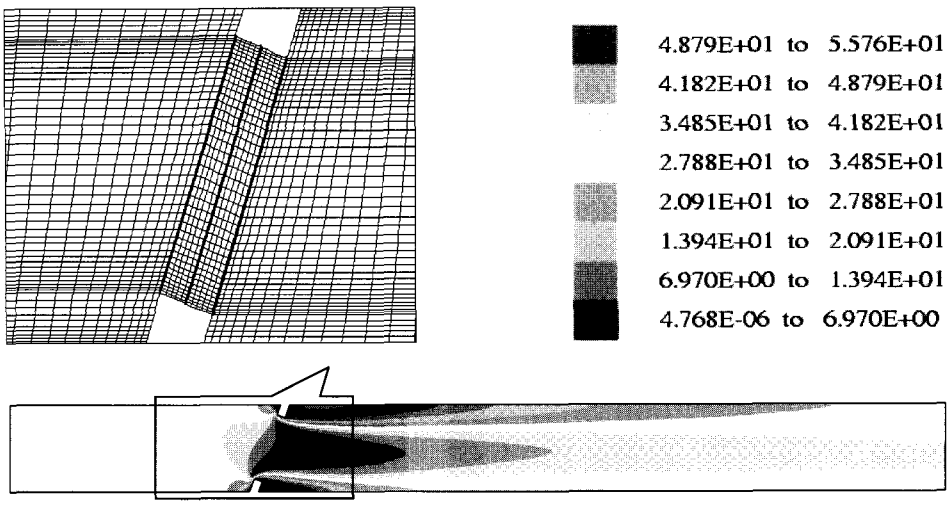

Fig. 3 Flow distributions and observation lines for double abutment cases

For the comparison of two different cases, the maximum velocity amplifications corresponding to each angle are shown in Fig. 4 along the 3 observation lines for both single and double abutment cases. From this figure, it can be seen that the maximum velocity amplifications are obtained for abutments placed perpendicular to the flow. The difference between maximum velocities corresponding to skewed single and double abutments can be up to 35 % and the difference is smallest for ϕ=90°, and increases with deviation from 90°.

Based on the values shown in Table 2, a nonlinear regression analysis was conducted to relate the maximum total velocity to skewness angle for different roughness values using a fixed projection ratio of σ=0.3. The coefficients of this relationship are shown in Table 3 with correlation coefficient γ^2.

The proposed velocity amplification can be derived from the nonlinear statistical analysis with skewness angle correction k_θ and is given as

$$\frac{U_{nose}}{U_{app.}} = \frac{\alpha F(\sigma, f)}{\left\{1+\left[\frac{(\theta-\beta)}{\gamma}\right]^2\right\}} = k_\theta F(\sigma, f) \tag{13}$$

where, θ = skewness angle in radians.

Table 3 gives the values of the function $F(\sigma, f)$ corresponding to the straight abutment case ($\theta = \pi/2$). From the Table 3, the parameter β increases in the direction of flow, going from upstream to downstream. Accordingly, maximum amplification takes place further downstream with increasing β. The parameter γcontrols the rate of variation of velocity amplification with angle; as its value increases, velocity variation with skewness angle becomes smaller.

This relationship can be combined with the equation derived by Molinas and Hafez (2000) for abutment nose velocity amplification for straight abutments. Molinas and Hafez related maximum velocity amplification to contraction ratio and the roughness factor according to

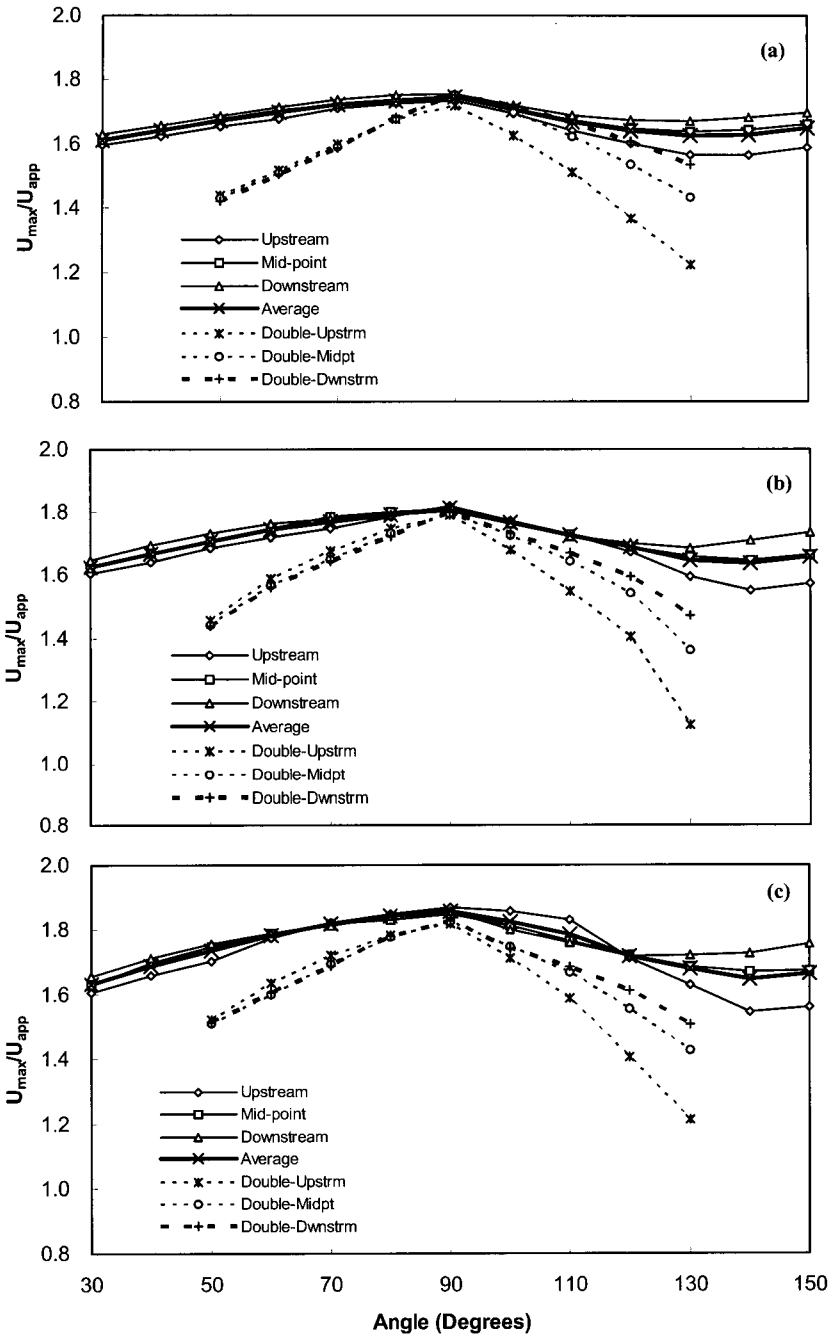

Fig. 4 Variation of velocity amplification with skewness: $f = 0.08$; (b) $f = 0.02$;(c) $f = 0.0088$

Table 3. Coefficients of Eq. (15) derived from nonlinear statistical analysis

f	Coefficients	Upstream	Mid-point	Downstream
0.08	$F(\sigma, f)$	1.5948	1.6134	1.6249
	α	1.06	1.06	1.06
	β	1.4649	1.5876	1.6648
	γ	1.3173	1.5308	1.6767
	r^2	0.9757	0.9670	0.9704
0.02	$F(\sigma, f)$	1.6806	1.6672	1.6619
	α	1.06	1.06	1.06
	β	1.4505	1.5438	1.5941
	γ	1.1562	1.3731	1.5126
	r^2	0.9700	0.9840	0.9820
0.0088	$F(\sigma, f)$	1.7061	1.6910	1.6861
	α	1.06	1.06	1.06
	β	1.4370	1.5287	1.5660
	γ	1.2300	1.4599	1.5967
	r^2	0.9845	0.9810	0.9652

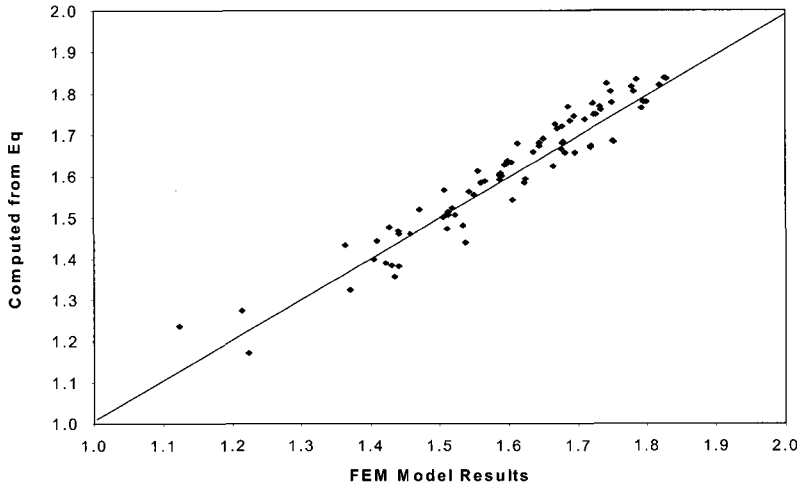

Fig. 5 Comparison of maximum velocities computed from the FEM model and from Eq. (15)

$$\frac{U_{nose}}{U_{app.}} = \frac{1-\sigma^2 \ln f/2}{1-\sigma} \quad (14)$$

where, U_{nose} is the total velocity at the abutment nose; $U_{app.}$ is the approach velocity at the channel inlet. Since U_{nose} for the 90°case represents $U_{\max}$ at the upstream, it is possible to replace U_{nose} with $U_{\max}$ which is the maximum velocity at the upstream, mid-point, and downstream along the abutment. The combined equation of Eq. (13) and (14) can be written as

$$\frac{U_{\max}(\theta)}{U_{app.}} = \frac{\alpha(1-\sigma^2 \ln f/2)}{1-\sigma}\left\{1+\left[\frac{(\theta-\beta)}{\gamma}\right]^2\right\}^{-1} \quad (15)$$

where θ = skewness angle in radians.

Values of the coefficients α, β, and γ for different roughness coefficients can be combined as follows.

Upstream: α= 1.06; β= 1.4508; γ= 1.2345
Mid-point: α= 1.06; β= 1.5534; γ= 1.4546
Downstream: α= 1.06; β= 1.6083; γ= 1.5953

The maximum velocity amplifications from the Eq. (15) and the results from the FEM model are compared in Fig. 5 using the above listed values of α, β, and γ. The agreement between Eq. (15) and the FEM model is very close and the deviation is within ±3 %.

5. SUMMARY AND CONCLUSIONS

As a conclusion for single abutment runs, up to 90°, the maximum velocities corresponding to the skewness angle proportionally increase with the angle increase. For the cases of the angle greater than 90°, the possible maximum velocities are little less than that of 90°. However, it shows little variation with respect to angle increase. The skewness angle effect is more significant for the double abutments regardless of the fact that the projection ratio is kept same for both cases. The findings from simulation runs on the two different abutment cases are summarized as follows

1. For single abutments, the projection ratio is the most significant factor for velocity amplifications. With constant contraction ratio, differences between the maximum velocities due to the skewness angle changes are less than 10%.
2. The skewness effect on the velocity amplification is more pronounced for the cases of double abutment. The corresponding difference between each of maximum velocity according to the angle variation is increased up to 30%.
3. The proposed Eq. (15) can be used to find approximate maximum velocities from provided skewness angles, roughness factors and the approach velocities.
4. For both of single and double abutment cases, peak velocities are obtained at 90°case.

REFERENCES

Berger, R. C. and Stockstill, R. L. (1995). "Finite-element model for high-velocity channels." *Journal of Hydraulic Engineering*, ASCE, Vol. 121 (10), pp. 710-716.

Brooks, A. N. and Hughes, T.J.R. (1982). "Streamline Upwind-Galerkin Formulations for Convection Dominated Flows with particular Emphasis on the Incompressible Navier-Stokes Equations." *Computer Methods in Applied Mechanics and Engineering*, Vol. 32, pp. 199-259.

Garmy, H. K., and Steffler P. M. (2002) "Effect of applying different distribution shapes for velocities and pressure on simulation of curved open channels" *Journal of Hydraulic Engineering*, ASCE, Vol. 128 (11), pp.

969-982.

Heinrich, J.C., Huyakorn, P.S., Zienkiwiewicz, O.C., and Mitchell, A.R., (1977). "An upwind finite element scheme for two dimensional convective transport equation." *International Journal for Numerical Methods in Engineering*, Vol. (11), pp. 627-643.

Katopodes, N. D. (1984). "A dissipative Galerkin scheme for open-channel flow." *Journal of Hydraulics Division*, ASCE, Vol. 110 (4), pp. 450-465.

Kwan, T. F. (1984). "Study of Abutment Scour." *University of Auckland School of Engineering Report No. 328,* Department of Civil Engineering, University of Auckland, Auckland, New Zealand.

Mayerle, R., Toro, F. M. and Wang, S. S. Y. (1995). "Verification of a three dimensional numerical model simulation of the flow in the vicinity of spur dikes." *Journal of Hydraulic Research*, Vol. (33), pp. 243-256.

Molinas, A., and Hafez, Y. (2000) "Finite Element Surface Model for Flow around Vertical wall Abutment." *Journal of Fluids and Structure*, Vol. (14), pp. 711-733.

Ouillon, S., and Dartus, D. (1997). "Three Dimensional Computation of Flow Around Groyne" *Journal of Hydraulic Engineering*, ASCE, Vol. 123 (1), pp. 962-970.

Rajaratnam, N., and Nwachukwu, B. (1983). "Flow Near Groyne-Like Structures." *Journal of Hydraulics Division*, ASCE, Vol. 109 (3), pp. 463-480.

Rastogi and Rodi (1978). "Predictions of heat and mass transfer in open channels." *Journal of Hydraulics Division*, ASCE, Vol. 104 (3), pp. 397-420.

Tisdale, T. S., Scarlatos, P. D. and Hamrick, J. M. (1998). "Streamline upwind finite-element method for overland flow." *Journal of Hydraulic Engineering*, ASCE, Vol. 124 (4), pp. 350-357.

Zienkiwicz, O. C. and Taylor, R. L. (1989) "The finite element method" 4th edition

---

Department of Civil Engineering, Colorado State University, Ft. Collins, Colorado, 80523 USA

(E-mail : hijnoh@empal.com)